symmetry

MDPI

Article

Angle-Resolved Lattice Population Density Plots: A Novel Approach for Fast 2D Unit Cell Determination from HAADF STEM Images

Thomas E. Weirich

Central Facility for Electron Microscopy, RWTH Aachen University, Ahornstr. 55, 52074 Aachen, Germany; weirich@gfe.rwth-aachen.de

Abstract: This study presents a new efficient method for determining the 2D unit cell size from HAADF STEM images using angle-resolved lattice population density (ALPD) plots. The approach uses the maxima in these plots, which represent the lines with the highest atom peak density, to determine the cell angle of the primitive 2D unit cell. Lattice types and 2D unit cell sizes that comply with crystallographic standards can easily be obtained by introducing angle constraints for the selection of the ALPD maxima. The method is very flexible and can be applied to images with fewer than 20 atom peaks, making it valuable for the automated analysis of periodic lattices in both large and small crystalline regions. The method has been evaluated for ideal and disordered lattices and is compared in terms of processing speed and the quality of results with the recently proposed real-space motif extraction method and with the well-established Fourier-based crystallographic image processing method commonly used for this task.

Keywords: HAADF STEM; 2D unit cell determination; motif extraction; crystallography; real-space method; automated analysis

Academic Editors: Marco Montemurro and Tomohiro Inagaki

Received: 3 November 2024
Revised: 27 January 2025
Accepted: 29 January 2025
Published: 6 February 2025

Citation: Weirich, T.E. Angle-Resolved Lattice Population Density Plots: A Novel Approach for Fast 2D Unit Cell Determination from HAADF STEM Images. *Symmetry* **2025**, *17*, 239. https://doi.org/10.3390/sym17020239

1. Introduction

High-resolution annular dark field (HAADF) scanning transmission electron microscopy (STEM) has become a key technique in materials science over the past two decades, providing atom-level insights essential for understanding and tailoring complex materials. The HAADF STEM signal of the atom columns in thin samples varies approximately between $Z^{1.5}$ and $Z^{1.7}$ [1], allowing not only for the visualization and determination of the symmetry of the periodic lattice but also for the measurement of the occupancy of atoms at specific sites [2]. Furthermore, HAADF image analysis allows the determination of deviations from the ideal lattice, such as defects, dislocations and interfaces, which can critically affect the mechanical, electrical and thermal properties of a material [3]. When the focus of HAADF image analysis is mainly on the periodic properties of the crystal lattice, it is common to describe it in terms of a 2D unit cell representing the basic motif of the periodic lattice. Thus, the initial step in analyzing the periodic lattice of an HAADF image is to determine the 2D lattice type [4,5] it belongs to and to determine the size of the 2D unit cell. As was shown for inorganic materials in the early 1990s, this goal can be easily achieved by using Fourier transforms and crystallographic image processing [6,7], for which several software packages exist e.g., [8,9]. However, recently, another method has been proposed for this task that automatically extracts motifs in real space by a variational approach using lattice projections [10]. A potential limitation of this approach for the automated analysis of HAADF images is the relatively high computational load, as it requires

the calculation of angle-resolved projections of a large number of atoms to determine the 2D cell geometry. In this contribution, it is shown that the goal of extracting the motif or 2D unit cell can be achieved with greater efficiency by exploiting the geometric properties of a single representative atom peak chosen in the HAADF lattice image. A comprehensive description of this complementary new approach using angle-resolved lattice population density plots is presented. In the following, the performance of the proposed method is tested on several examples with different lattice geometries and numbers of atoms and is compared with other available methods.

2. Materials and Methods

2.1. Calculation of Angle-Resolved Lattice Population Density (ALPD) Plots

The method proposed here is based entirely on the geometric analysis of the 2D positions of the projected atom columns in an HAADF image of a crystalline region, which are assumed to be known. For simple monoatomic structures, where all 2D lattice nodes at the four corners are occupied by an atom, the first step in the calculation is to select an arbitrary atom peak in the HAADF image as the origin, and then to sum all other atom peaks as a function of the angle around the atom peak in the center (Figure 1). This RADAR-like process yields the angle-resolved lattice population density $H(\varphi)$ (Equation (1)). Here, φ denotes the rotating angle around the atom selected as the origin, φ_i is the angle of the line relative to the zero angle of the coordinate system with atom i (dotted line in Figure 1) and $\Delta\varphi$ denotes half the step size used for increasing the rotating angle. The last variable also defines the angular resolution of the obtained lattice population density plot.

$$H(\varphi) = \sum_{i=1}^{n} \delta\,;\ \varphi = 0\ \ldots\ \pi;\ \delta = \left\{ \begin{array}{c} 0:\ |\varphi_i - \varphi| > \Delta\varphi \\ 1:\ |\varphi_i - \varphi| \ \leq\ \Delta\varphi \end{array} \right\} \tag{1}$$

The 2D lattice vectors $\vec{a}$ and $\vec{b}$ of the 2D unit cell are then given by the shortest distances Δ between the selected atom in the center and the next atom along each of the lines with the highest lattice population density (see Figure 1) according to

$$\vec{a} = (\Delta x_a,\ \Delta y_a)\,;\ \vec{b} = (\Delta x_b,\ \Delta y_b) \tag{2}$$

The corresponding 2D unit cell angle γ is obtained from Equation (3).

$$\gamma = \arccos\left(\frac{\vec{a} \cdot \vec{b}}{\left|\vec{a}\right| \cdot \left|\vec{b}\right|} \right) \tag{3}$$

As can be seen in Figure 1, the directions of the two lattice axes of the 2D unit cell (shown in orange) from the origin correspond to the red and green lines with the highest atom density within the analyzed circle. For a perfect regular lattice, the length of the two unit cell axes is defined by the distance of the two nearest atoms from the origin, and the cell angle is given by the difference between the positions of the two corresponding maxima in the ALPD plot in Figure 2. The following main conclusions can be drawn from this straightforward geometric analysis:

- The angle difference between the two largest maxima in the ALPD plot (lines with the highest atom density) of a monoatomic structure defines the cell angle of the primitive 2D unit cell.

- For a perfect regular primitive lattice, with atoms at all lattice nodes, the lengths of the two axes of the primitive unit cell are given by the distances of the two closest atom peaks along each line to the atom at the origin.

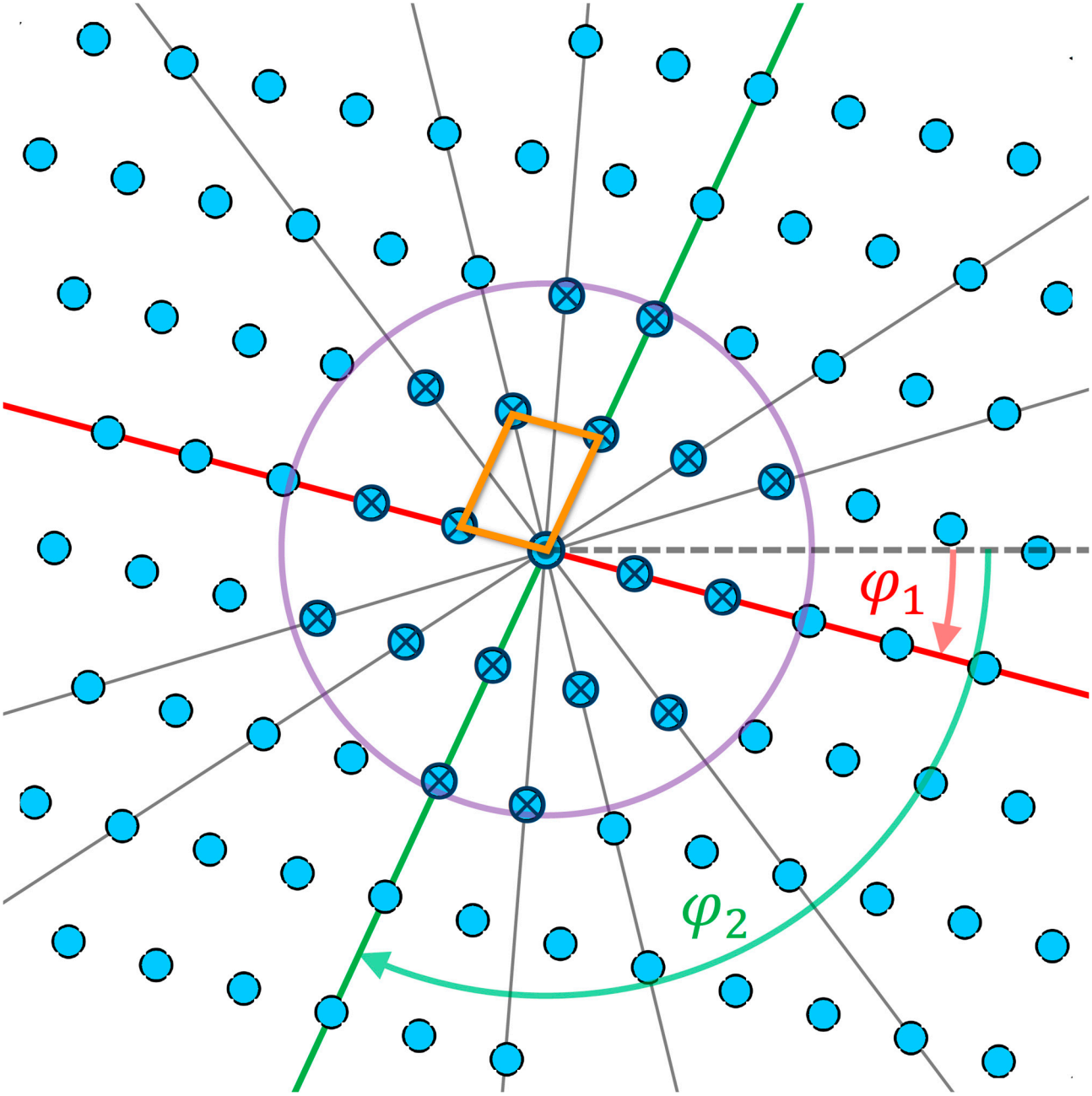

Figure 1. The principle for obtaining the angle-resolved lattice population density of an oblique 2D lattice. In this RADAR-like method, within a predefined range from the origin, the number of atoms along the line with angle φ is summed. In the example shown above, there are 18 atoms (marked by ⊗) in total surrounding the atom at the center within the shown boundary circle. Of these, there are 4 atoms each along the red and green lines, which correspond to the two maxima in the ALPD plot in Figure 2. As can be seen in the figure above, the direction of the two lattice axes of the 2D unit cell (shown in orange) corresponds to the red and green lines with the highest atom density within the boundary circle. For a perfect regular lattice, the 2D unit cell angle is defined by the angle between the two nearest atoms from the origin on these lines and can be obtained directly from the plot in Figure 2.

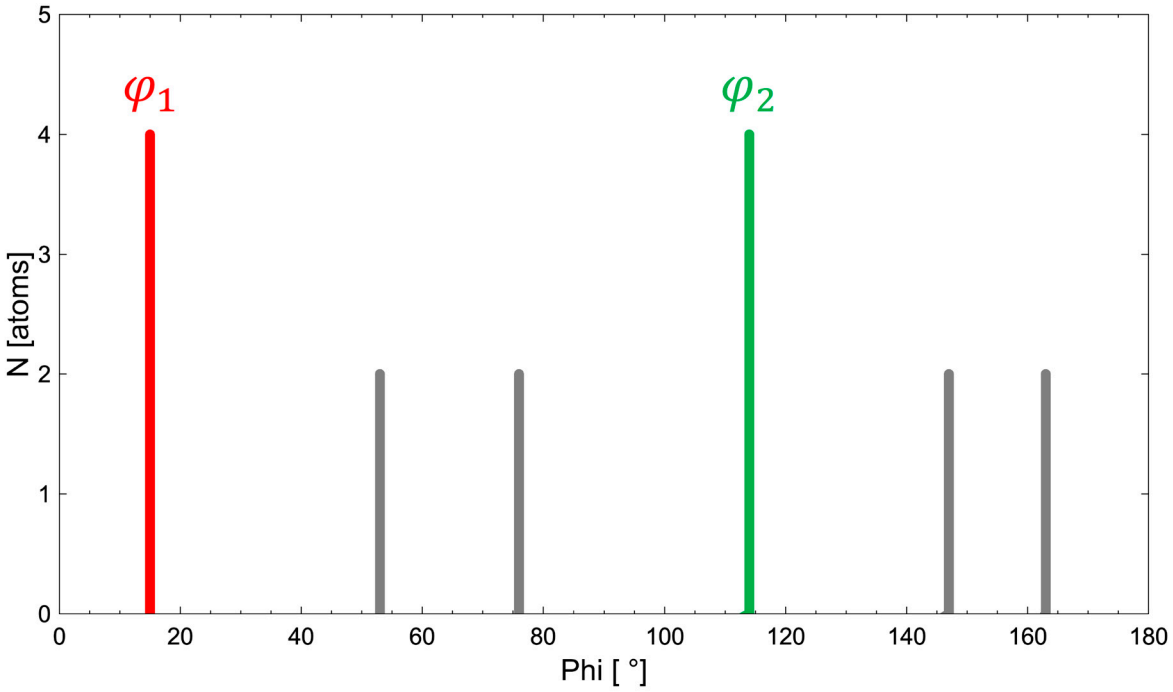

Figure 2. The ALPD plot obtained for the oblique 2D lattice in Figure 1 within the defined boundary circle. Note that the red and green maxima in the plot at 15° and 115°, each with 4 atoms, correspond to the lattice lines with the shortest atom distances to the center atom. The distances from the center atom at the origin to each of these nearest atoms are equal to the lattice parameters of the primitive 2D unit cell, and the corresponding cell angle is given by the angle difference of the two maxima in the above plot.

2.2. Test Images and Software

To test the general validity of these conclusions, a series of monoatom pseudo-HAADF images with different 2D lattice geometries was generated using the structure visualization software VESTA (Version 3) [11]. As these are only artificially generated point patterns for testing, without reference to an actual crystal structure, the distances determined during the analysis are given in pixel units. Before processing, the resulting structure images were blurred with a Gaussian filter to make them more similar to real HAADF images. The 2D atom positions were then determined using ImageJ's (Version 2.16.0/1.54 g) [12]. *Find Maxima* function and saved for later use. The actual analysis of the atom peaks was carried out by means of a macro program in ImageJ, which works according to the principle described above. The macro program is highly automated, as it can self-select the atom peak with the maximum possible boundary radius from the image, calculate the ALPD plots, and calculate the 2D unit cell at the selected origin and draw it into the pseudo-HAADF image. Some of the parameters can also be defined by the user, such as the user's own atom peak as the origin, the bounding circle around the atom peak at the origin, and the minimum angular difference between the maxima in the ALPD plots used to calculate the 2D cell angle. The minimum distance between two accepted maxima in the ALPD plots was set to 85° by default in the calculations presented here, unless otherwise stated. As a result, only unit cells that comply with the crystallographic convention of legal cell angles greater than 90° are obtained. In addition, a peak intensity discriminator function for handling non-monoatom lattices has been implemented, which allows the selection of peak intensity ranges for analysis. The main characteristics of the pseudo-HAADF images that were used to test the basic functionality of the program are summarized in Table 1.

Table 1. Characteristics of the used monoatom pseudo-HAADF images for testing the proposed method.

2D Lattice Type	Plane Group Symmetry	Number of Peaks Within Maximum Circle	Figure #
Oblique P	*p*2 (no. 2)	593	Figures 3 and 4
Rectangular P	*p*2*mm* (no. 6)	672	Figures 5 and 6
Rectangular C	*c*2*mm* (no. 9)	1576	Figures 7 and 8
Hexagonal P	*p*6*mm* (no. 17)	2267	Figures 9 and 10
Square P	*p*4*mm* (no. 11)	929	Figures 11 and 12

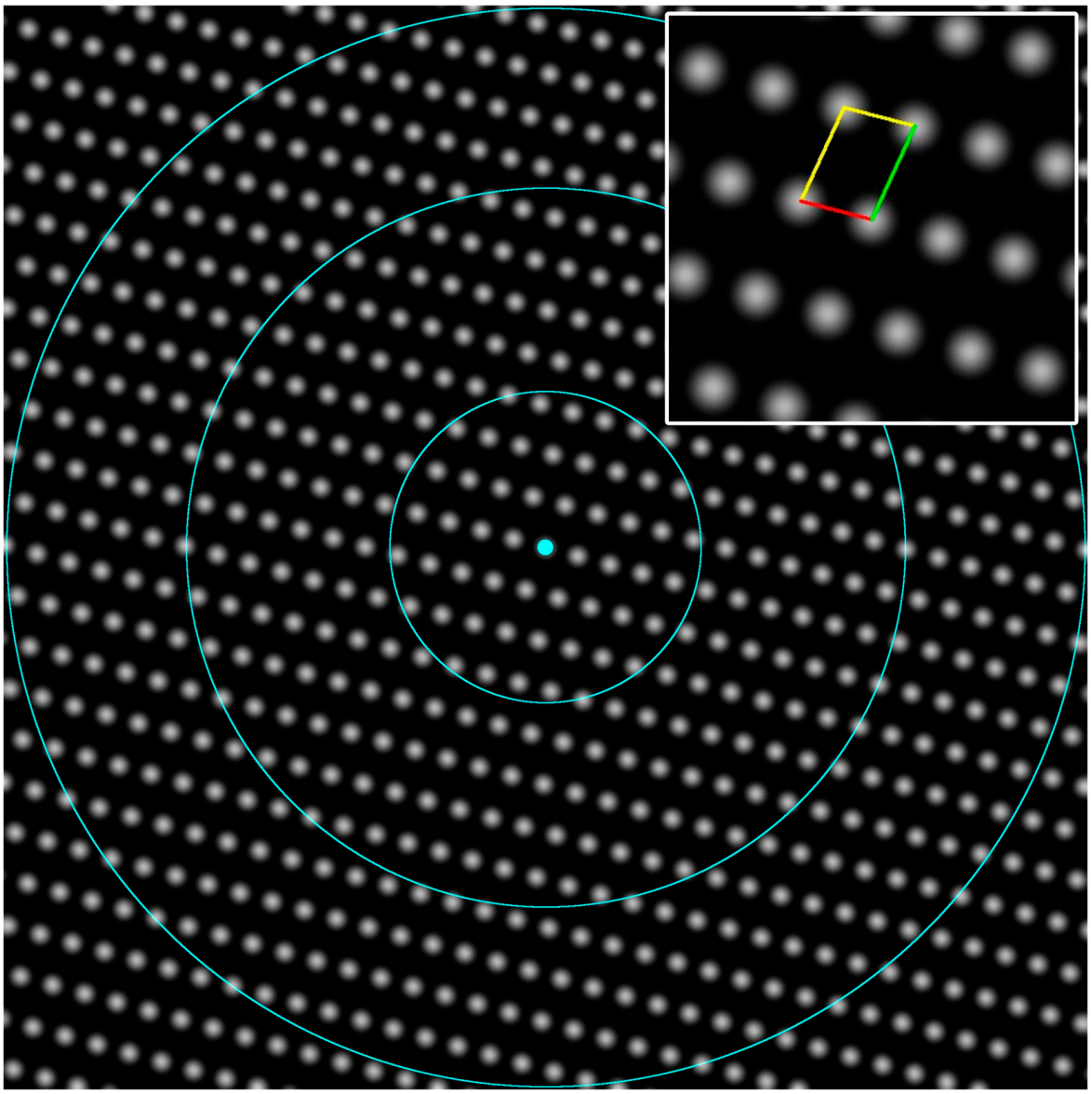

Figure 3. Oblique P lattice used to follow the evolution of the ALPD plots shown in Figure 4 with the increasing number of atom peaks. The number of atom peaks analyzed for calculating the ALPD plots was 50 (in the inner circle), 260 and 593 (within the largest circle). The determined unit cell was, in all cases, the one shown in the inset with a(red) = 71.3 pixels, b(green) = 100.2 pixels and γ = 100.2° since the last variable is always calculated from the positions of the closest atom peaks to the marked atom at the origin.

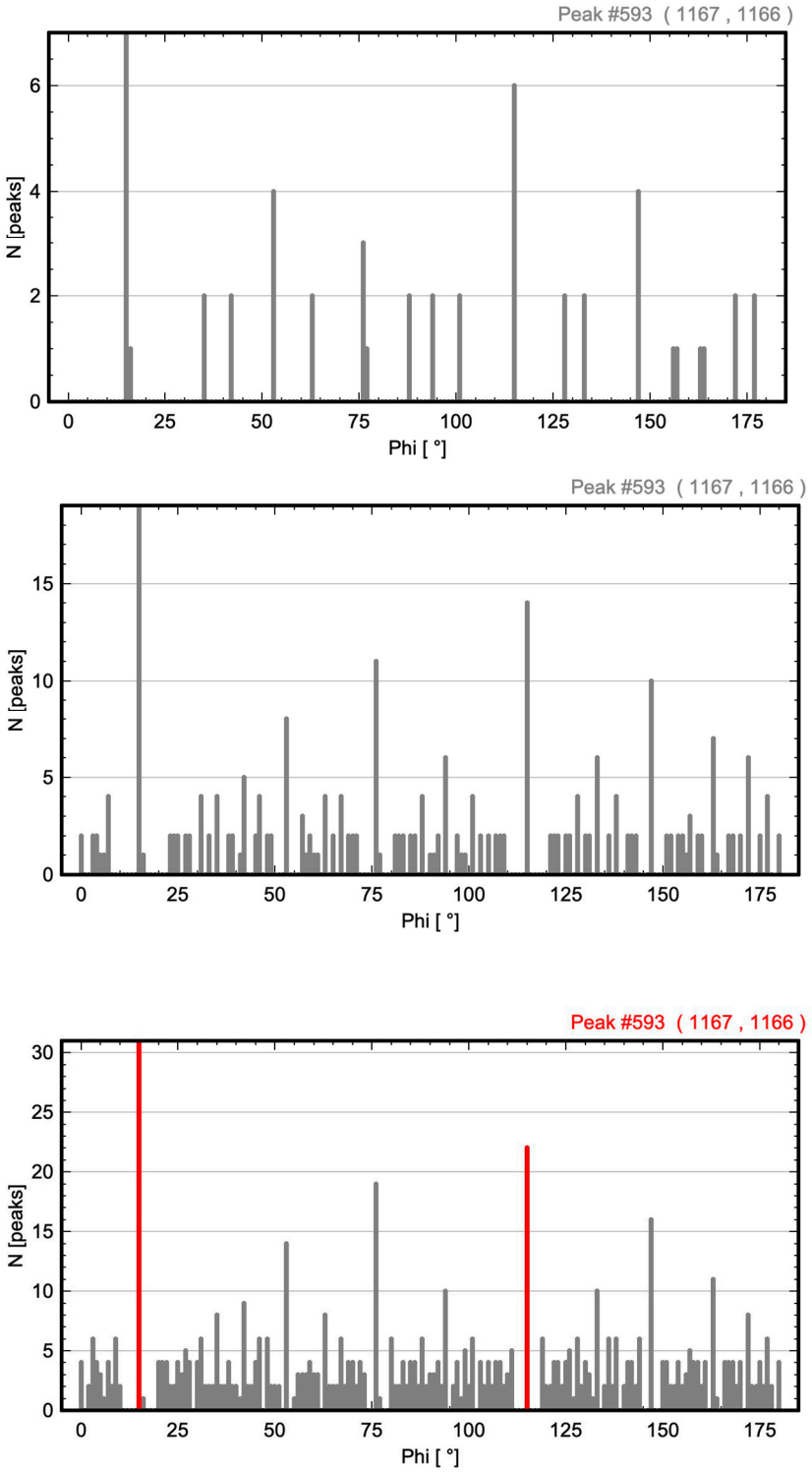

Figure 4. The evolution of the ALPD plots with the increasing number of atom peaks. The number of atom peaks analyzed was 50, 260 and 593 from top to bottom. The plots clearly show that the two strongest peaks, marked in red in the bottom figure, with the highest atom density remain the strongest for both small and large numbers of atom peaks. It should also be noted that for large numbers of atoms, the maxima at angles 15° and 115°, representing the prominent cell axes, are characterized by pronounced empty regions with zero counts on both sides of the maximum.

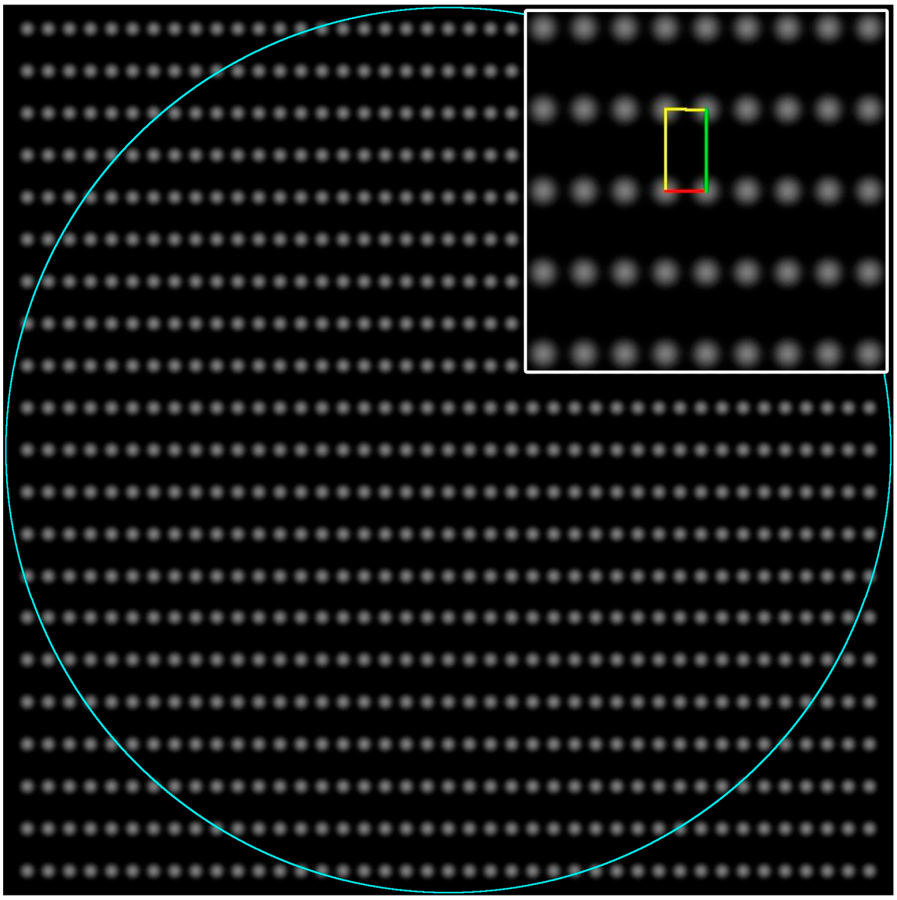

Figure 5. The rectangular P lattice used for calculating the ALPD plot in Figure 5. The calculation was performed with 672 atom peaks within the shown circle with a radius of 948 pixels. The determined 2D unit cell of *a*(red) = 45 pixels, *b*(green) = 90 pixels and $\gamma = 90°$ is shown in the inset.

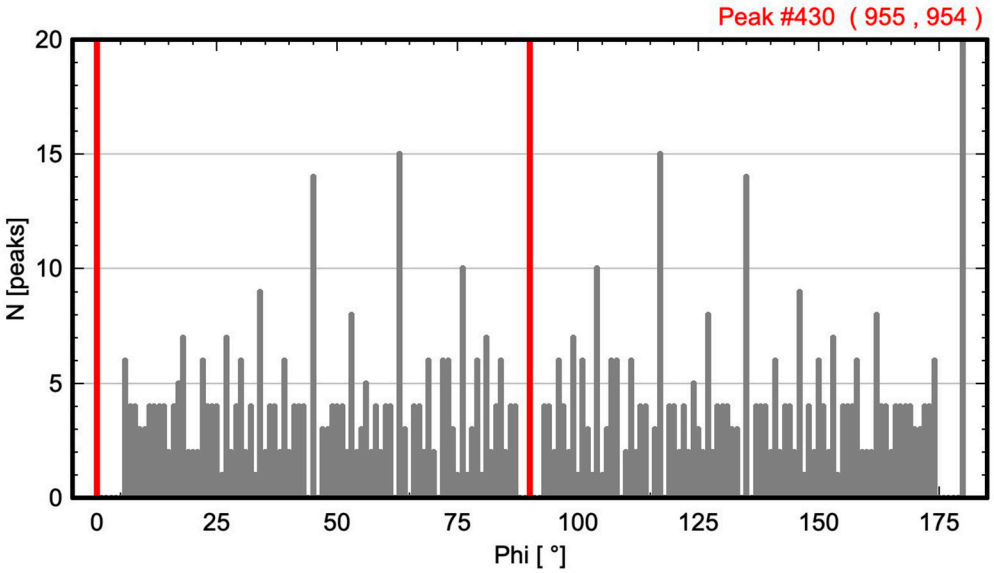

Figure 6. The ALPD plot for the rectangular P lattice shown in Figure 5. The maxima marked in red at angles 0° and 90° relate to the cell axes, and their angular difference determines the 2D unit cell angle. Note the empty regions with zero counts on the sides of the maxima, which is a characteristic feature of the principal cell axes.

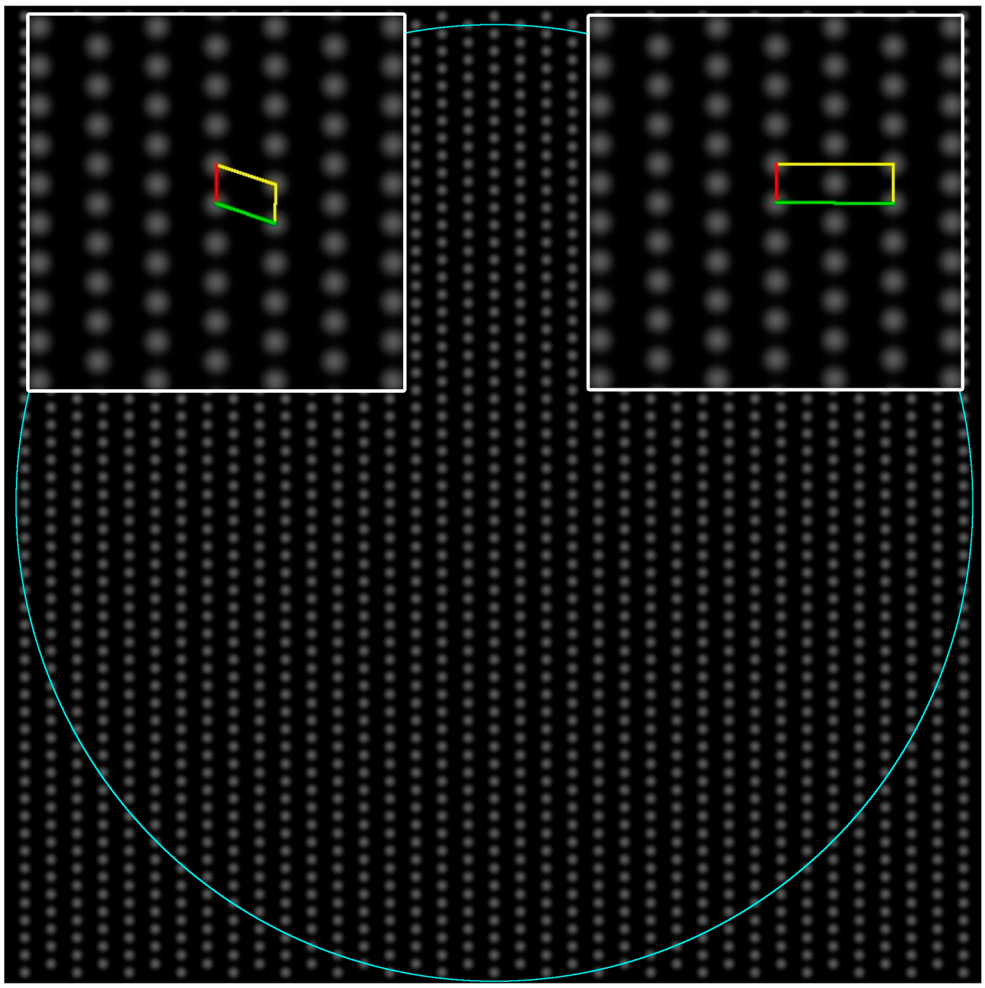

Figure 7. The rectangular C-centered lattice used for calculating the ALPD plots in Figure 8. The calculations were performed with 1576 atom peaks within the shown circle with a radius of 1151 pixels. The primitive 2D unit cell (inset on the left) has the lattice parameters a(red) = 41 pixels, *b*(green) = 65.5 pixels and $\gamma = 108.7^{\circ}$. The corresponding lattice parameters for the true C-centered lattice, after enforcing that only angular maxima separated by at least 85° are considered, are a(red) = 41 pixels, b(green) = 125 pixels and $\gamma = 90.5^{\circ}$.

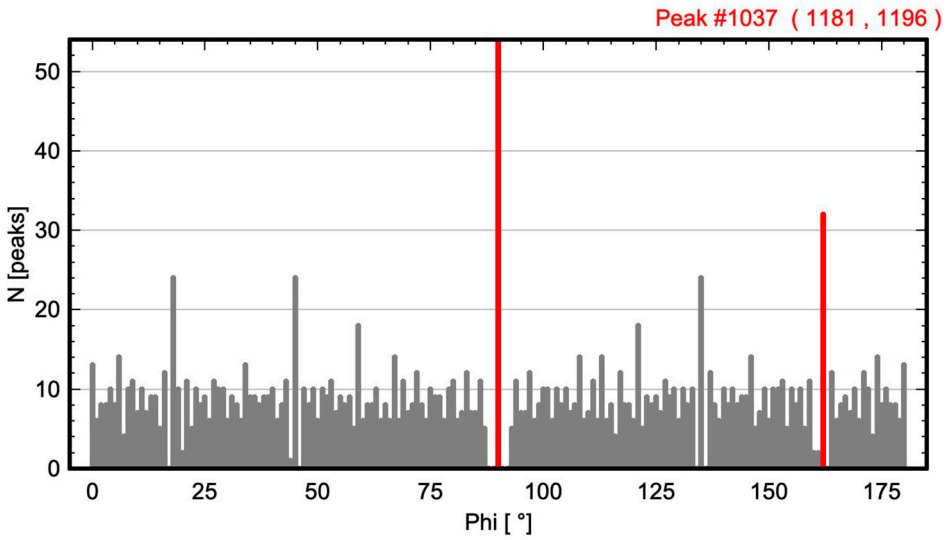

Figure 8. *Cont.*

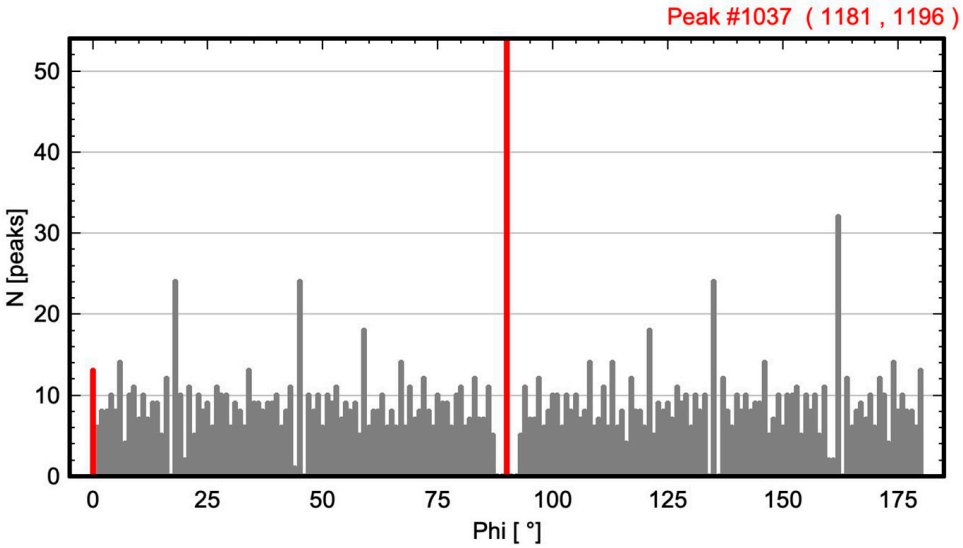

Figure 8. ALPD plots for the rectangular C-centered lattice shown in Figure 7. The maxima in red in the upper plot at 90° and 162° are those taken automatically by the program for calculating the primitive unit cell (see Figure 7). The determination of the (true) C-centered cell could be enforced by setting the minimum angular difference between two maxima to 85°, so the red-marked maxima at angles 0° and 90° were taken to derive the cell angle. The empty regions with zero counts on the sides of the maximum at 90° clearly indicate that this must be one of the main cell axes for both cell types. The gap to the left of the maximum at 162° indicates that this angle refers to the preferred second axis. However, crystallographic rules require the larger C-centered cell to be chosen if 90° cell angles are possible.

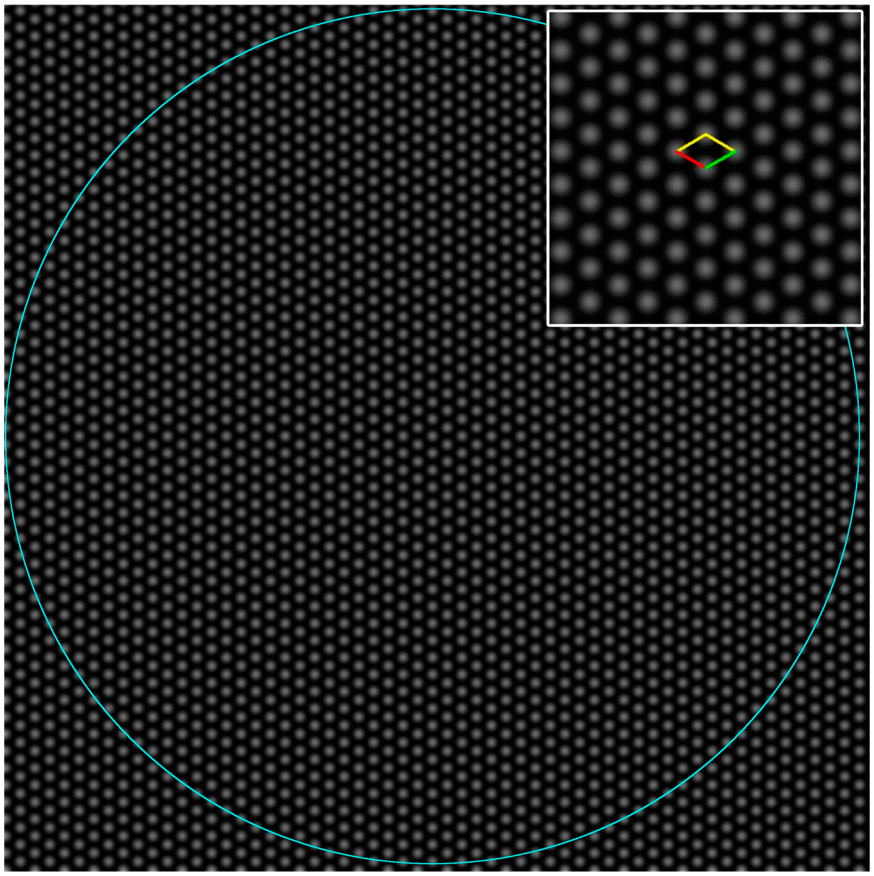

Figure 9. The hexagonal P lattice used for calculating the ALPD plots in Figure 10. The calculations were performed with 2267 atom peaks within the shown circle with a radius of 1072 pixels. The primitive 2D unit cell (inset) has the lattice parameters a(red) = 42.5 pixels, b(green) = 42.5 pixels and γ = 120.8°.

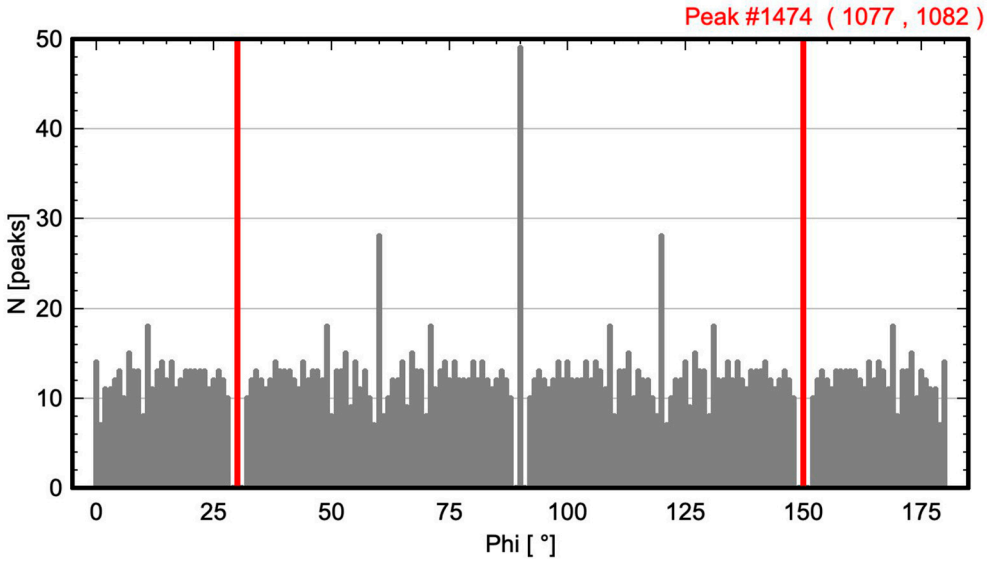

Figure 10. The ALPD plot for the hexagonal P lattice shown in Figure 9. The maxima marked in red at angles 30° and 150° refer to the conventional hexagonal cell axes with a cell angle of 120°. The latter was forced to be chosen by setting the minimum angular difference between the two maxima to be used to 85°. As in the other cases, the empty spaces with zero counts on the sides of the maxima indicate that they relate to the main cell axes. Note that the orthohexagonal cell would be obtained if the maxima at 30° (50 counts) and 120° (28 counts) were chosen.

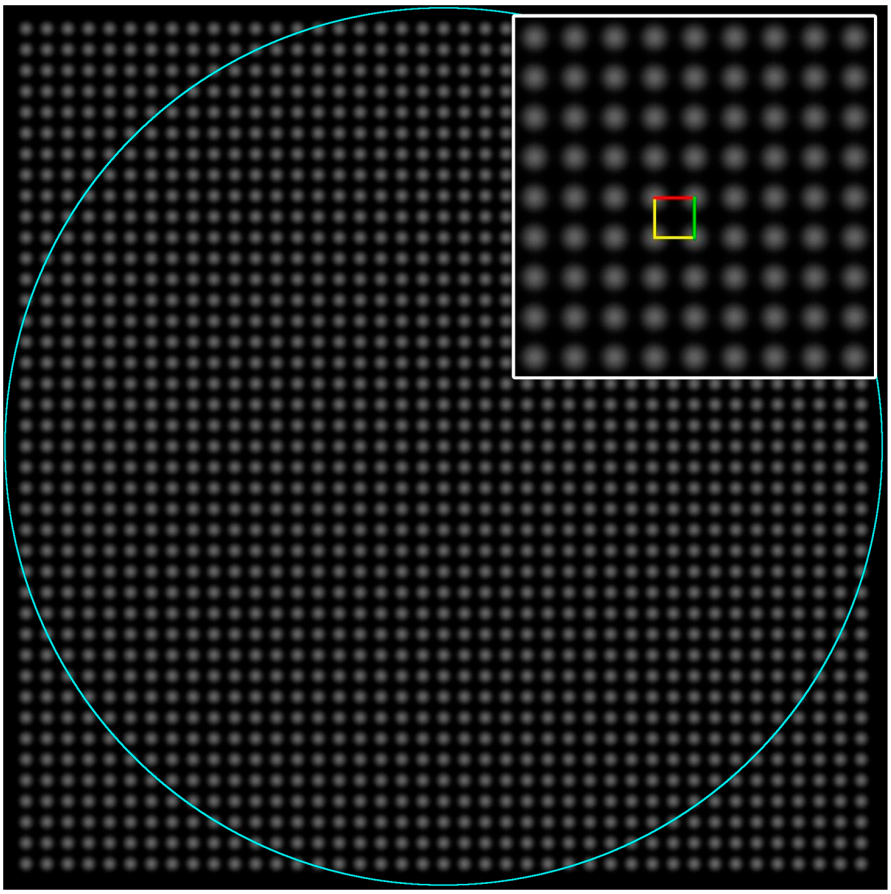

Figure 11. The square P lattice used for calculating the ALPD plots in Figure 12. The calculations were performed with 1350 atom peaks within the shown circle with a radius of 929 pixels. The primitive 2D unit cell (inset) has the lattice parameters a(red) = 44 pixels, b(green) = 44 pixels and $\gamma = 90°$.

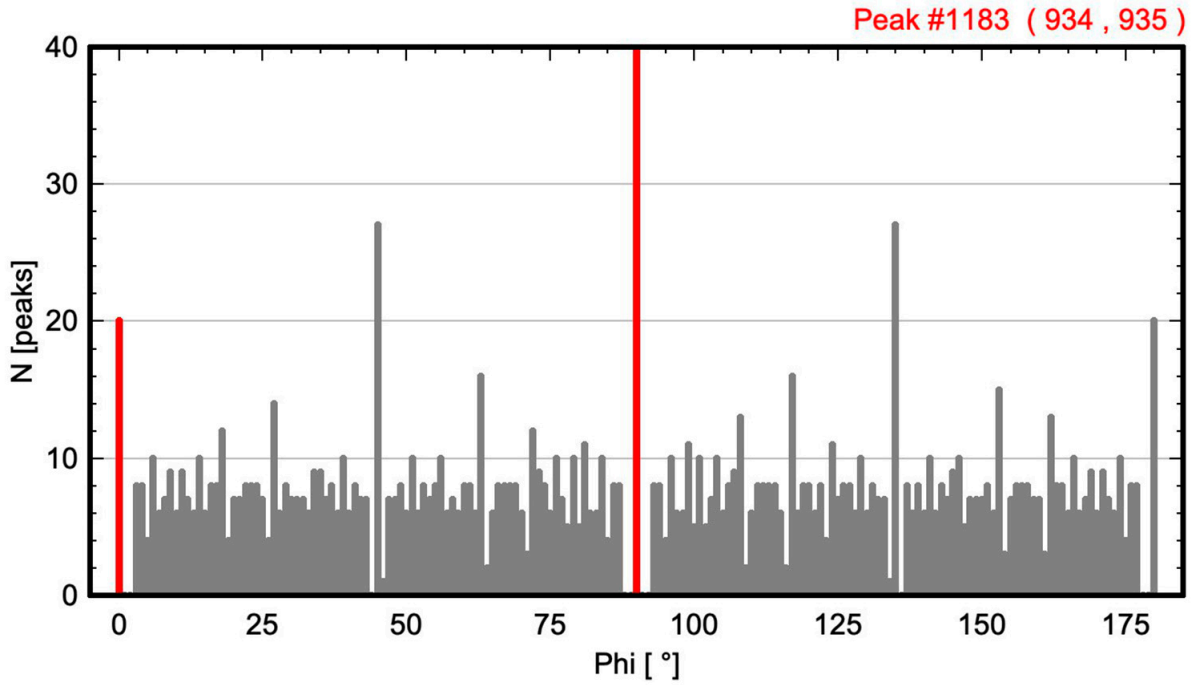

Figure 12. The ALPD plot for the square P lattice shown in Figure 9. The maxima marked in red at angles 0° and 90° refer to the conventional 90° cell angles. Again, the latter was forced to be chosen by setting the minimum angular difference between the two maxima to be used to 85°. As in the other cases, the pronounced empty spaces with zero counts on the sides of the maxima indicate that they relate to the main cell axes. Note that a unit cell with a = 44 pixels, b = 62.2 pixels and γ = 45° would have been obtained by choosing the maxima at 90° (40 counts) and 135° (27 counts). However, as mentioned for the rectangular lattice (Figure 8), crystallographic rules require that the cell be chosen with 90° cell angles if possible.

2.3. Lattices of Real Crystal Structures

2.3.1. Magnesium

Whereas the hexagonal test structure in Figure 9 with plane group symmetry *p6mm* represents a monoatomic face-centered cubic (fcc) structure projected along one of the <111> directions, true hexagonal closed-packed (hcp) monoatomic structures, such as that formed by magnesium [13], have no atoms at positions with 6-fold symmetry projected along the [001] direction. According to crystallographic rules, the positions with 6-fold symmetry also mark the unit cell origin and the other three 2D unit cell corners. This, however, causes problems for the proposed method since it assumes that all corners of the primitive 2D unit cell are occupied by atoms. To handle the hexagonal case, a module has been implemented in the program that performs the required shift of the 2D unit cell origin if hexagonal symmetry is detected. If the position of the central atom peak is defined as the origin of the coordinate system and $\vec{a}$ and $\vec{b}$ are the lattice vectors that point to the two neighbor atoms of the central atom, the origin of the true 2D hexagonal cell is obtained from the shift vector $-\vec{b}$. Correspondingly, the new lattice vectors are defined as $\vec{a'} = 2\vec{a} + \vec{b}$ and $\vec{b'} = \vec{b} - \vec{a}$ (see Figure 13).

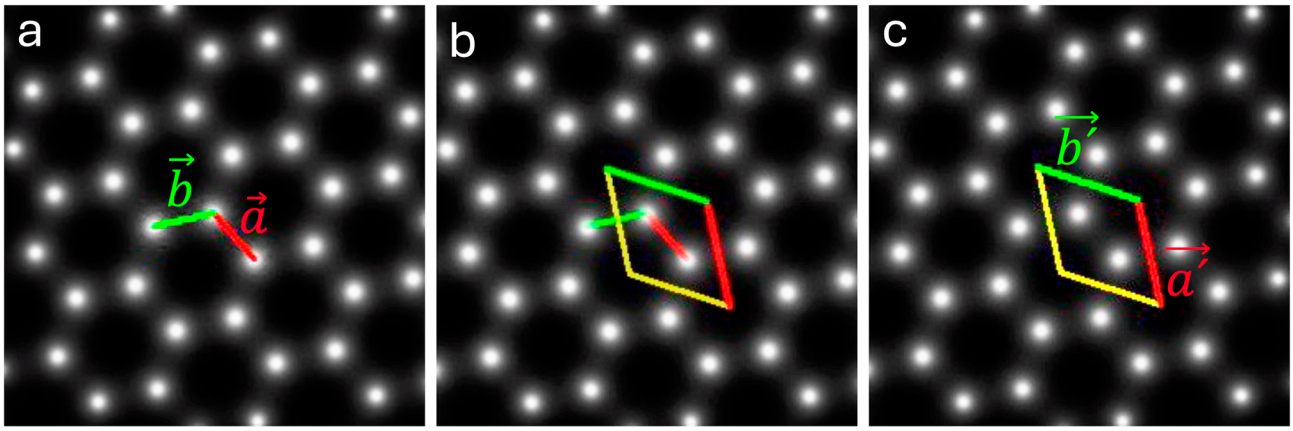

Figure 13. The determination of the 2D unit cell for the regular hexagonal closed-packed (hcp) structure of magnesium using the ALPD plot in Figure 14. The initial unit cell dimensions, as determined from the nearest atom peaks to the central atom, are a(red) = 37.5 pixels (1.854 Å) and b(green) = 36.9 pixels (1.825 Å). The corresponding cell angle, as determined from 405 atom peaks around the central atom, is $\gamma = 120°$. Since the algorithm of the developed program expects all cell edges to be occupied by atoms, the found unit cell in (**a**) is identified as a pseudo-solution. As the determined cell angle suggests a hexagonal cell, the new cell shown in (**b**), of twice the size is then calculated, which agrees with the crystallographic convention to place the unit cell origin at a position with 6-fold symmetry. As illustrated above, the true hexagonal unit cell is obtained by shifting the unit cell origin from the position of the central atom in (**a**) toward the center of the upper-right hexagon that is formed by 6 atom peaks in (**b**,**c**). The corresponding shift vector for the unit cell origin is $-\vec{b}$, and the lattice vectors of the new cell are $\vec{a'} = 2\vec{a} + \vec{b}$ and $\vec{b'} = \vec{b} - \vec{a}$. Using the values obtained for the pseudo-solution yields a'(red) = 64.2 pixels (3.174 Å), b'(green) = 65.5 pixels (3.239 Å) and γ' = 120.5° for the true cell. Averaging the lattice parameters finally gives a' = 64.9 pixels (3.207 Å) and γ' = 120° for the hexagonal 2D unit cell.

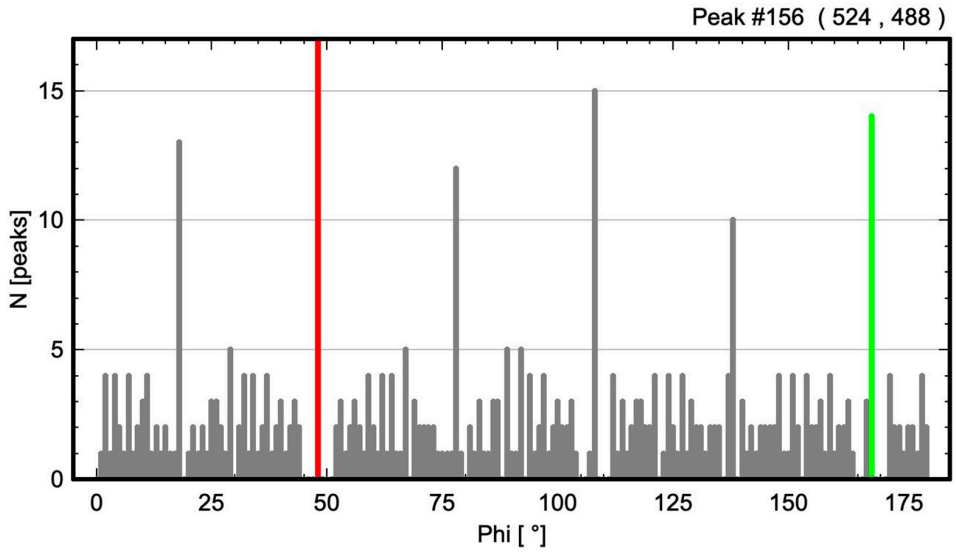

Figure 14. The ALPD plot for the regular hexagonal closed-packed (hcp) structure of magnesium in Figure 13 using a circular ROI around the central atom peak of about 24 Å (483 pixels) containing 405 atom peaks. In this case, the program was allowed to find the unit cells with cell angles between 96° and 125° and an angular error of 2°. The program-determined 2D unit cell angle is 120°, as calculated from the difference between the maxima at 48° and 168°, respectively. The peaks marked in red and green refer to the determined unit cell axes of the same color in Figure 13. Note that the initially found unit cell is a pseudo-solution, as described in detail in the text and the figure caption of Figure 13.

2.3.2. Barium Titanium Oxide, $BaTiO_3$

As proved by the analysis of the 2D point lattices listed in Table 1, the investigated approach can identify and retrieve the underlying motif (2D unit cell) of simple structures when the atom peaks are located on a regular lattice. To check whether this approach is robust enough to also work on distorted and more complex structures, the following test scenario was established. For this, the JEMS program [www.jems-swiss.ch (accessed on 2 November 2024)] was employed to calculate [001]-projected potential maps for disordered and perfect ordered ideal cubic barium titanate, $BaTiO_3$ [14], which then served as surrogates for HAADF images. For the distorted structures, all projected atom peaks were allowed to relocate randomly in-plane from their original positions between 6 and 15 pixels, which corresponds to atom peak displacements between 0.36 and 0.89 Å, respectively (Table 2). For calculating the ALPD plots, only the strongest peaks, which refer to the projected barium atoms, were considered since they are located on the edges of the undistorted projected 3D unit cell in the B-type setting of perovskite structures [15]. The selection of the strong peaks for the analysis was achieved by using the peak intensity discriminator function mentioned in Section 2.2. Moreover, in the search for the second-strongest peak in the ALPD plots, the program was advised to select only those that yield the cell angle closest to 90°. This constraint was applied to obtain comparable results and to avoid other solutions with larger or smaller cell angles. The within this test are shown in Figure 15, and the processed pseudo-HAADF images with the maximum populated lattice directions used for calculating the cell angles in Table 2 are shown in Figure 16.

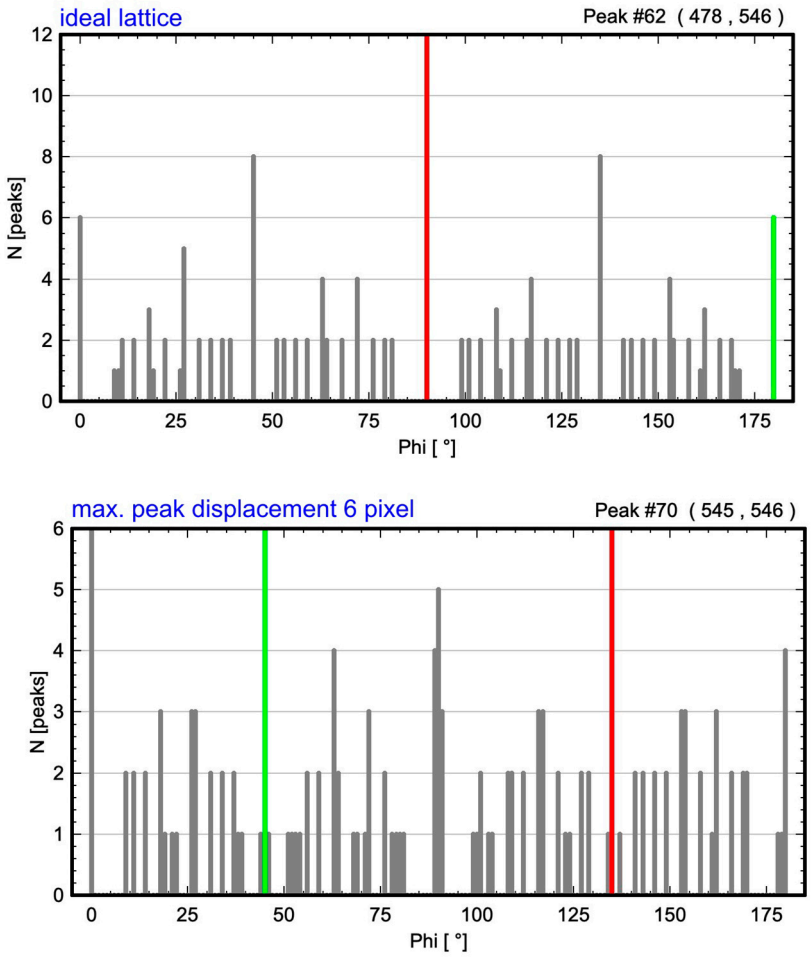

Figure 15. *Cont.*

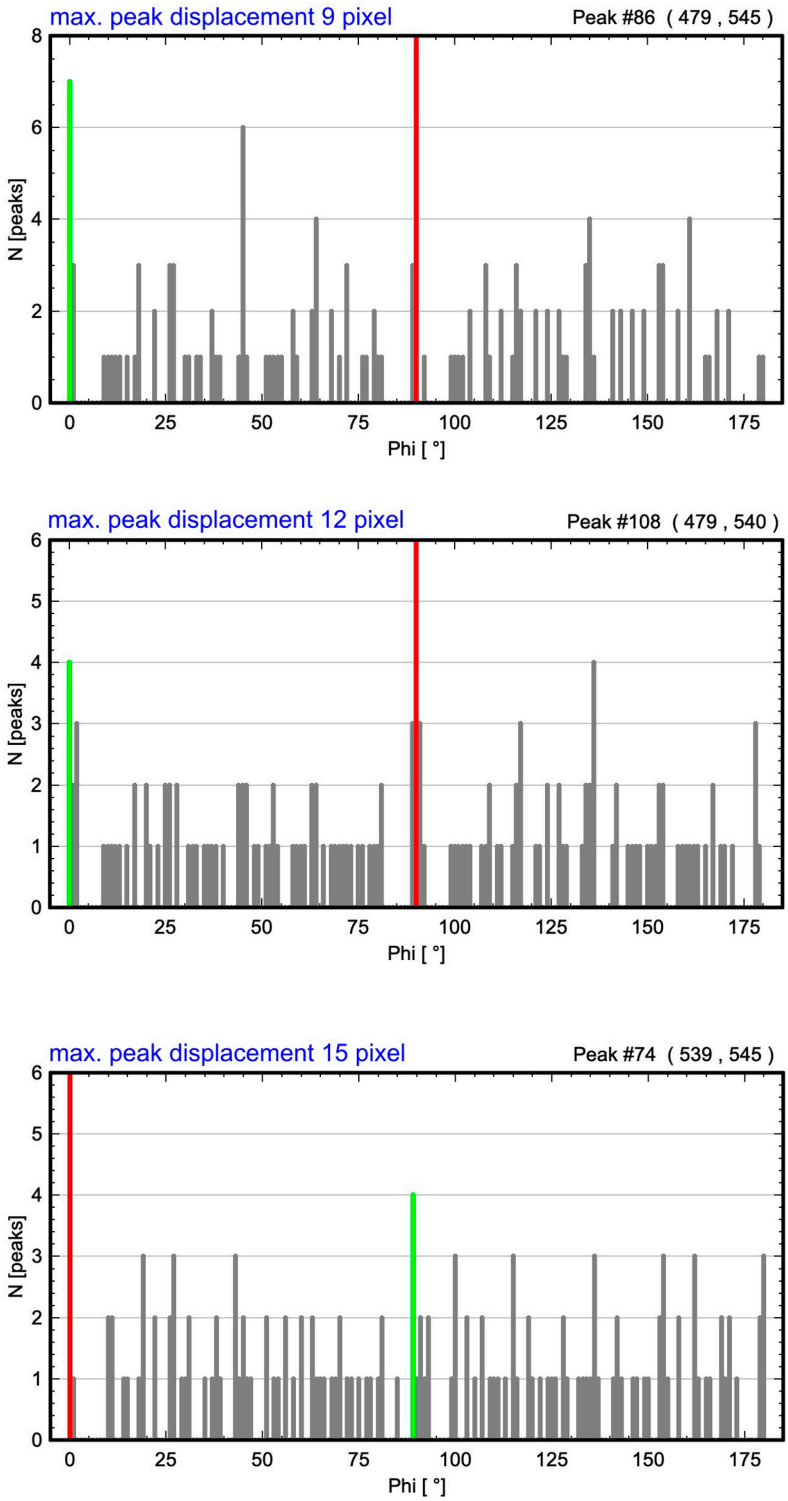

Figure 15. The evolution of the ALPD plots for cubic $BaTiO_3$ with increasing random atom peak displacements. Peaks marked in red and green refer to detected directions of same color with highest atom population in Figure 16.

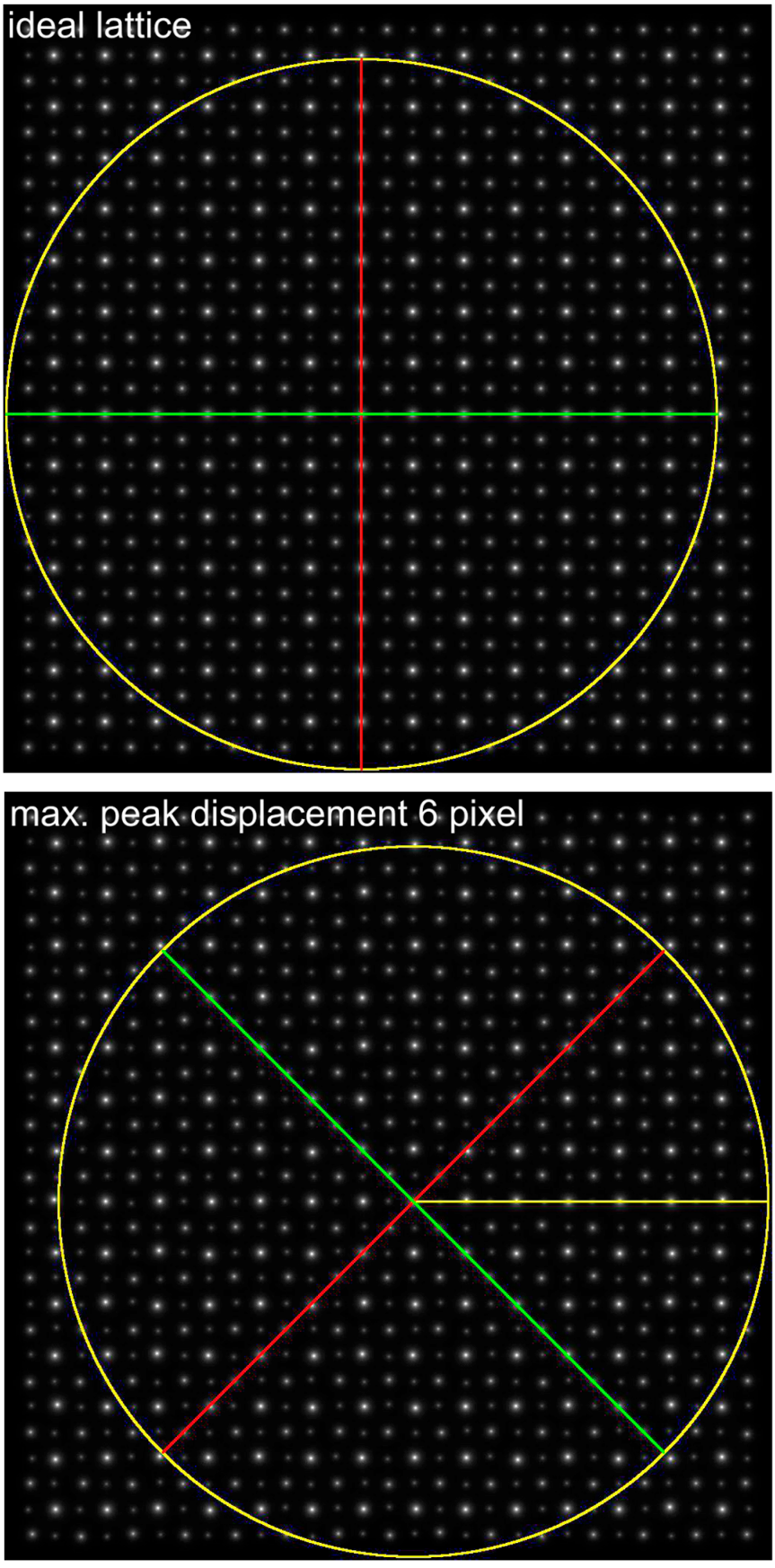

Figure 16. *Cont.*

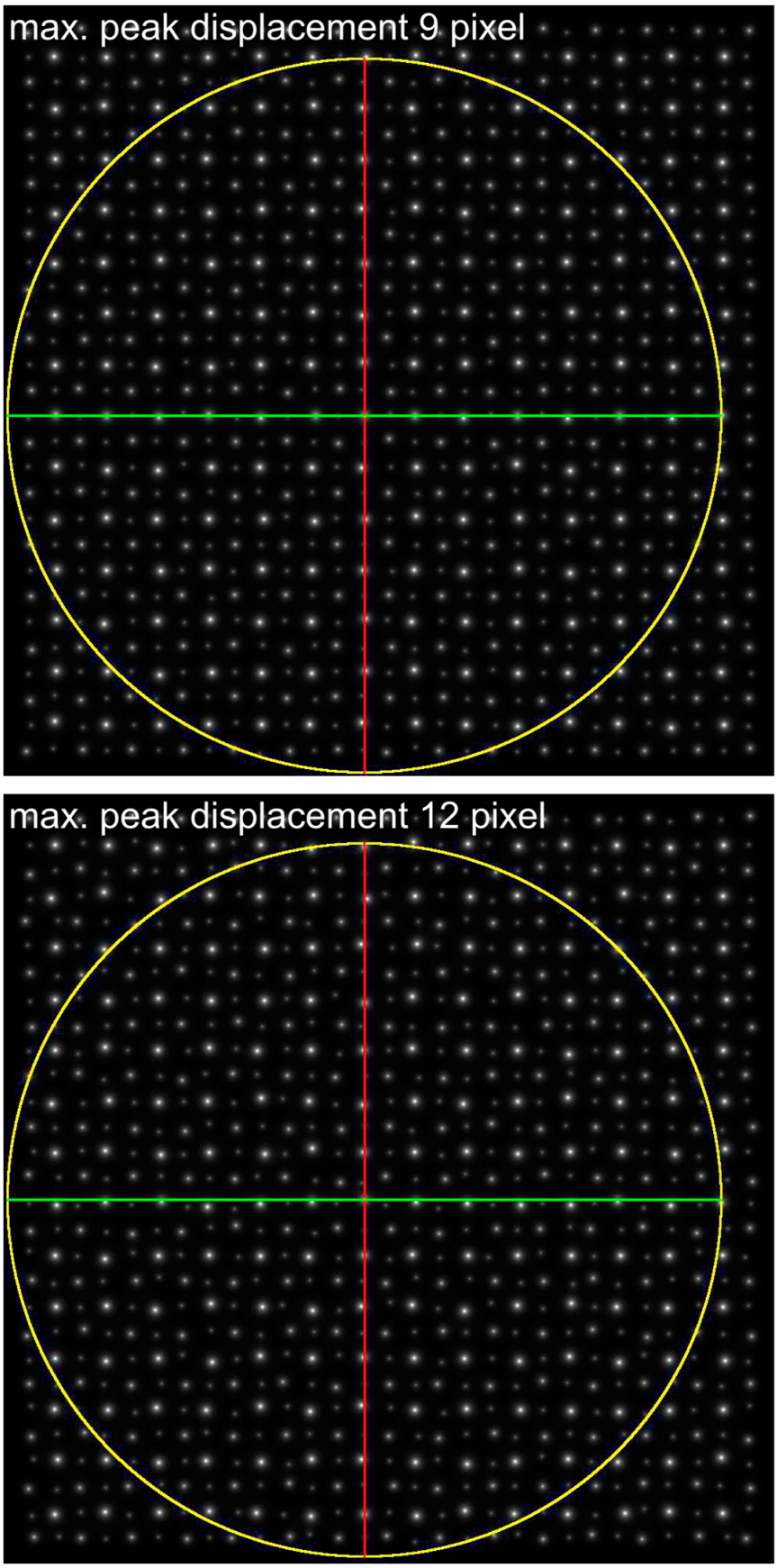

Figure 16. *Cont*.

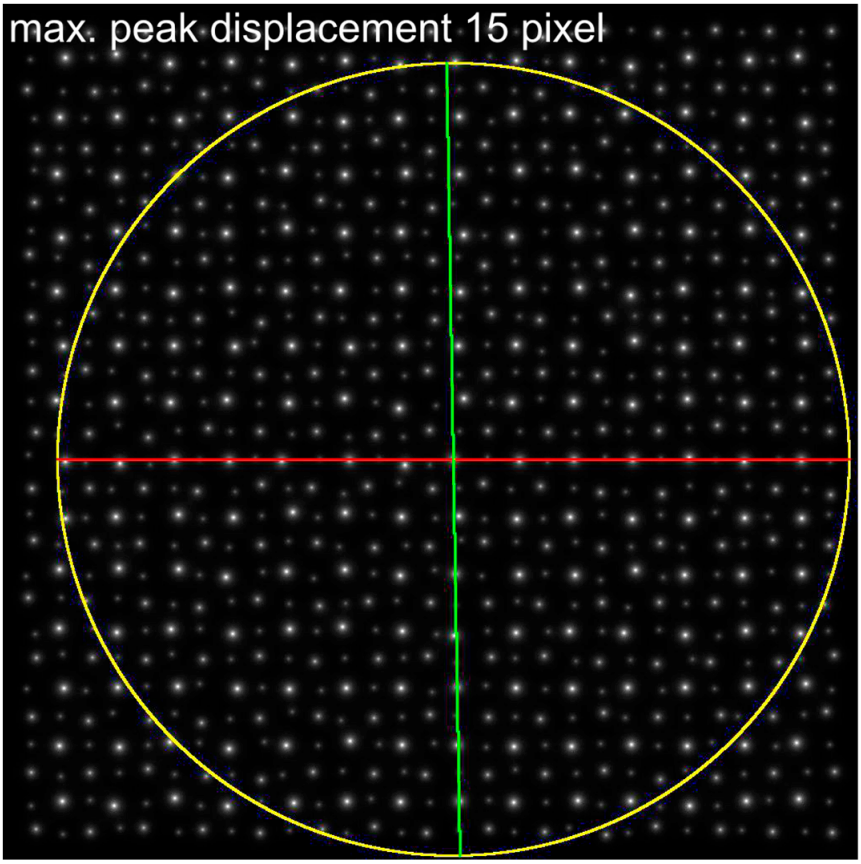

Figure 16. Projected potential maps of $BaTiO_3$ with increasing in-plane atom peak displacements used for calculating the ALPD plots in Figure 15. The superimposed yellow circle marks the maximum considered distance of atom peaks to the center peak. The red and the green lines are the lines with the maximum population when the expected 2D unit cell angle is allowed to vary between 85° and 95°, and only the strong barium peaks are analyzed.

Table 2. The 2D lattice characteristics of the used [001]-projected structures of $BaTiO_3$ with different degrees of atom peak displacements.

Maximum Atom Peak Displacement in Pixel	Maximum Atom Peak Displacement in Å	Number of Analyzed Atom Peaks for Barium Within Maximum Circle	1st Maximum (Red) at Angle	2nd Considered Maximum (Green) at Angle	Determined Cell Angle from ALPD Plot
0	0	144	90°	180°	90°
6	0.36	144	135°	45°	90°
9	0.53	144	90°	0°	90°
12	0.71	148	90°	0°	90°
15	0.89	146	0°	89°	89°

2.4. Comparison with Fourier-Based Crystallographic Image Processing (CIP)

As mentioned in Section 1, the task of determining the 2D unit cell dimensions and atom positions from HR(S)TEM images of inorganic materials can be easily achieved by using Fourier transforms and crystallographic image processing (CIP) [16–18]. For benchmarking purposes, the pseudo-HAADF images of ideal and disordered $BaTiO_3$, with a maximum peak displacement of 12 pixels (0.71 Å), were analyzed by both methods. Crystallographic processing of the pseudo-HAADF images in Figure 17 was performed using CRISP version 2.2 from Calidris [9]. The results of this processing are summarized in Figure 18. Figure 19 shows the corresponding results obtained using ALPD plots on the same images.

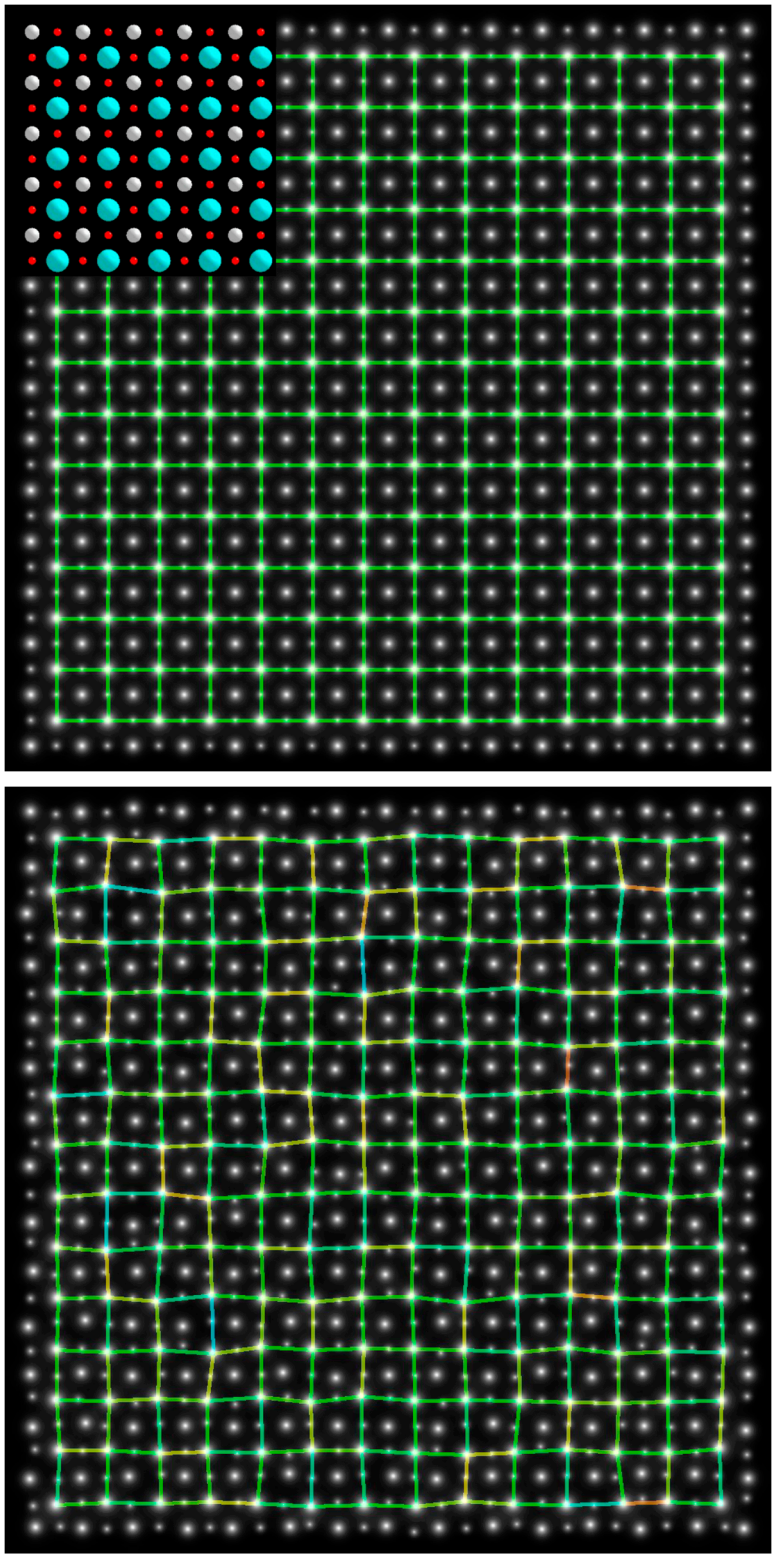

Figure 17. Ideal and disordered projected potential maps of $BaTiO_3$ along the [001] direction used for the benchmark test of the ALPD and CIP methods. The upper map shows, in the inset, the projected structure of the ideal lattice of cubic $BaTiO_3$ with barium atoms in green–blue, oxygen in red and the mixed position of titanium and oxygen in gray. For illustration of the regularity of the lattice, a grid has been overlaid on the projected potential map that shows barium at all lattice node positions. The map at the bottom shows the corresponding projected potential map after random peak displacements for all atoms up to 12 pixels off from their ideal position. Enlarged Ba-Ba distances are marked in blue, and shortened Ba-Ba distances are marked by yellow–orange grid lines.

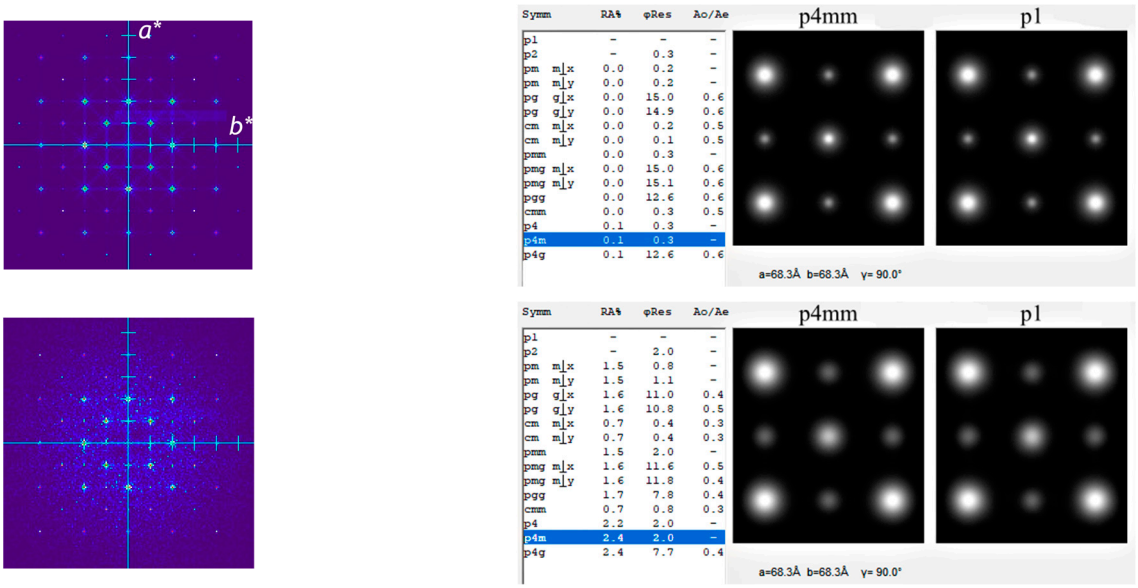

Figure 18. Crystallographic image processing of the ideal (**top**) and disordered projected potential maps (**bottom**) of the pseudo-HAADF images of $BaTiO_3$ in Figure 17 with the program CRISP [9]. As shown by the averaged maps on the right, both the p1 and phase-corrected p4mm maps yield essentially the same size and geometry of the 2D unit cell for the ideal and disordered lattices ($a = b = 68.3$ pixels $\cong 4.05$ Å, $\gamma = 90°$). The random displacement of atom peaks is, however, responsible for the slightly larger residuals for the amplitudes (RA%) and phases (**φ**Res), the less sharp atom peaks in the averaged maps and the visible loss in resolution in the Fourier transforms on the left. Moreover, the introduced disorder generates some diffuse background with a few additional peaks between the maxima of the ideal reciprocal lattice.

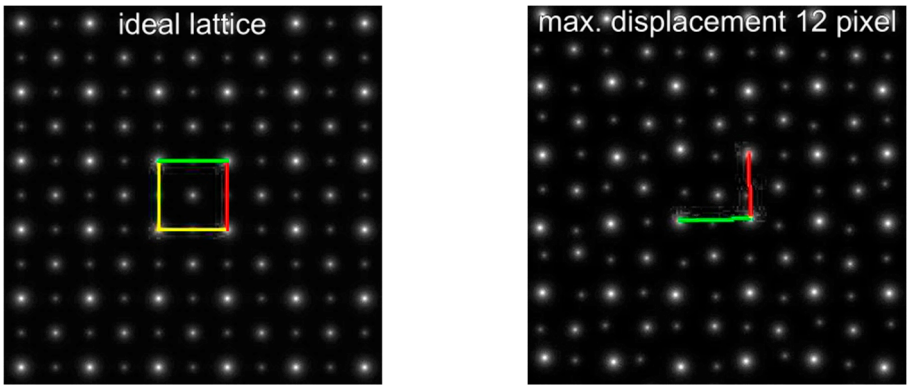

Figure 19. Results from processing the pseudo-HAADF images of $BaTiO_3$ in Figure 17 using ALPD plots. Even though a 90° rectangular lattice was clearly detected for both cases in the first step of the analysis (see Table 2 and Figure 16), a complete unit cell could only be recovered for the ideal periodic lattice on the left. The 2D unit cell dimensions determined from the nearest peak positions to the analyzed central atom (=cell origin) for the ideal structure are a(red) = b(green) = 68 pixels $\cong$ 4.03 Å, $\gamma = 90$ °. The determined principal axes for the disordered structure with allowed peak displacements of up to 12 pixels (0.71 Å) are a(red) = 64 pixels $\cong$ 3.80 Å, b(green) = 70 pixels $\cong$ 4.15 Å and $\gamma = 90.7°$.

2.5. Comparison with the Real-Space Approach Using Lattice Projections

Alhassan and co-workers [10] have recently proposed a new method for automatic motif extraction in real space from the lattice projections of HAADF images of crystalline materials. The authors tested their method on several synthetic and experimental HAADF-STEM images, including images of trigonal Nb_7Co_6 [19], for which the primitive 2D unit cell along the [110] direction was determined. As this was the most complex structure

treated in their report, it was used here to check whether the ALPD approach developed in this study would give the same results.

Again, the first step was to use the JEMS program [www.jems-swiss.ch (accessed on 2 November 2024)] to generate a projected potential map of the structure projected along the [110] direction, which was then processed with the ALPD program using only the strongest peaks in the cobalt sublattice and the constraint that only cell angles greater than 93° are considered. The resulting ALPD plot and 2D unit cell are shown in Figures 20 and 21.

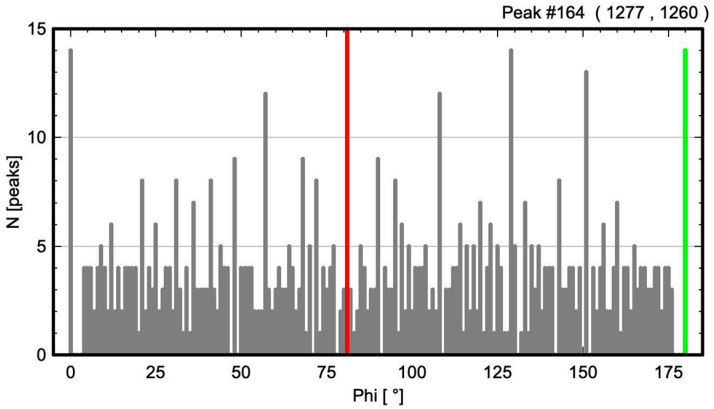

Figure 20. The ALPD plot for trigonal Nb_7Co_6 [19] projected along the [110] direction. The plot was calculated using a circular ROI around the central atom peak of 1238 pixels containing 671 strong cobalt peaks. In this case, the program was allowed to find unit cells with cell angles between 93° and 123° and an angular error of 2°. The 2D unit cell angle determined by the program is 99°, calculated from the difference between the maxima at 81° and 180°.

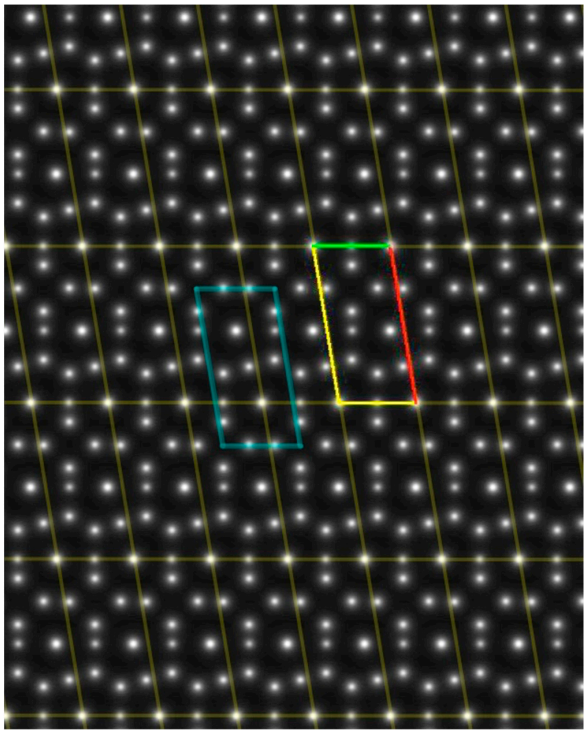

Figure 21. A pseudo-HAADF image of trigonal Nb_7Co_6 [19] projected along the [110] direction. The unit cell and periodicity determined by the ALPD approach in this study and the corresponding unit cell obtained by Alhassan and co-workers [10] are shown as an overlay. As can be seen, both unit cells match in size and orientation and represent legal 2D unit cells for this projection. The ALPD cell, determined from the peak positions around the cell origin, has the dimensions a(red) = 173.3 pixels, b(green) = 84 pixels, γ = 99.3°.

3. Results

3.1. Oblique P Lattice

To follow the changes in the ALPD plots with the increasing number of atom peaks, three different boundary radii were placed around the atom peak near the center of the image (Figure 3), and the corresponding plots were calculated (Figure 4). The plots clearly show that the two largest maxima with the highest atom density remain the strongest for both small and large numbers of atom peaks. It is also important to note that for large numbers of atoms, the maxima at angles 15° and 115°, representing the prominent cell axes, are characterized by empty regions with zero counts on either side of them.

These findings confirm the earlier statement that the angle difference between the two strongest maxima in the ALPD plot (lines with the highest atom density) defines the cell angle of the 2D unit cell, independent of the size of the area analyzed. The 2D unit cell determined was, in all cases, the one shown in the inset of Figure 3, which is calculated from the closest atom peaks along the red and green lines to the atom at the origin.

3.2. Results from Testing the Higher Symmetry Lattices

The analysis of the other 2D lattices listed in Table 1 is consistent with the result obtained for the oblique lattice: i.e., the angles related to the main cell axes are characterized by pronounced maxima with empty regions with zero counts on either side (see Figures 6, 8, 10 and 12). In all cases, the maxima corresponding to the principal axes are found among the two strongest peaks with the highest atom population density of the lattice (Figures 4, 6, 8, 10 and 12). It should be emphasized that the unit cell angles derived from the two strongest maxima yield valid primitive unit cells in all cases, which can be used as a basic motif to represent the entire periodic lattice of the 2D structure. However, the unit cells derived from the two strongest maxima do not necessarily conform to the crystallographic rules for choosing a unit cell, i.e., the requirement for 90° cell angles for the rectangular and square lattices and a 120° cell angle for the hexagonal lattice type [4,5]. In order to comply with these rules, the mechanism for selecting the second maximum for the cell angle determination needs to be managed. For the automatic mode of the developed program, introducing the restriction to skip the second-largest maximum if the angle difference is less than 85° degrees was sufficient to arrive at the (crystallographically) correct 2D unit cell for the rectangular C-centered lattice (Figures 7 and 8), the hexagonal P lattice (Figures 9 and 10) and the square P lattice (Figures 11 and 12). Despite this formal drawback, which can easily be fixed by imposing angular constraints, the tests performed for the five possible 2D lattice symmetries demonstrate that the 2D unit cell can be quickly and reliably retrieved by calculating the ALPD plot for any single-atom peak in a periodic monoatomic lattice.

3.3. Results from Testing Lattices of Real Crystal Structures

As the test on real structures showed, the analysis with ALPD plots requires, in some cases, treating some symmetries with additional constraints, such as in the rectangular and hexagonal cases, or selecting sublattices for non-monoatomic structures to obtain useful results. As demonstrated for the hcp magnesium test case (Section 2.3.1), the code to detect and handle these special cases can be easily implemented in the program to allow automatic or semi-automatic processing. The selection of sublattices for non-monoatomic structures is also likely to be suited for automation, but this has not been attempted at this stage, as it is crucial to set the peak intensity limits correctly for the method to work properly. However, as demonstrated for the barium sublattice of $BaTiO_3$ (Section 2.3.2), the true 2D unit cell is straightforwardly obtained if the constraints for a square lattice and the limits of the implemented peak intensity discriminator function have been set correctly. In this context,

it should be noted that the first constraint is also a potential subject for full automation, as it is characterized by peak maxima with a 45° difference in the ALPD plot, which are easily detectable (see Figures 12 and 15). While the analysis of 2D lattice images with ALPD plots works reliably for identifying the complete basic motif of an ideal lattice, comparison with Fourier-based crystallographic image processing, CIP (Section 2.4), showed that ALPD was only partially successful when applied to images of structures with significant random atom displacements from their ideal positions. Since the Fourier-based CIP method, like X-ray diffraction, treats the lattice as a whole and therefore always provides an averaged result, random structural disorder will only cause the peak intensities to become more blurred and smeared around the ideal position, as shown in Figure 18. The determined 2D unit cell, the desired structural motif, however, remains unaffected. The basic idea behind the ALPD method, as described in Section 2.1, is, however, that each atom peak is a true representative of the entire lattice (or sublattice), as illustrated by the example of the barium atoms in the top map in Figure 17. The lattice parameters can then be calculated from the distances of the two nearest atoms to any atom defined as the origin, regardless of which atom was selected as the central atom. As shown by the ALPD results for disordered $BaTiO_3$ in Figure 19, introducing notable atom peak displacements removes the basis of this concept, and it is no longer possible to define a valid 2D unit cell, since all calculated base vectors represent only the local distance in two directions around a selected central atom (for illustration, see the bottom map in Figure 17). Nevertheless, the ALPD method may still be successfully applied to real HAADF images of perovskite-type ceramics, since experimentally determined temperature factors of crystal structures indicate that the actual atom displacements in crystalline samples are at least an order of magnitude smaller than in the scenario simulated here [20]. Despite the lack of usefulness of ALPD for processing structurally disordered images, it is noteworthy that the ALPD method was still able to recover the cell angles of the underlying structure without atom disorder (see Table 2).

4. Discussion

HAADF STEM is commonly used to image the projected lattices of rather simple crystal structures formed by atom columns that are aligned along a low-index zone axis (e.g., <001> or <110> in the case of cubic materials). Irrespective of the crystal orientation that has been chosen for imaging, the lattice will fall into one of the five possible 2D lattice categories listed in Table 1. Accordingly, the first step in analyzing the periodic lattice of an HAADF image is to first determine the 2D lattice type it belongs to and, second, determine the size of the 2D unit cell. The angle-resolved lattice population density (ALPD) method developed here and implemented as an ImageJ macro script has proven to be fast and reliable for both tasks. As shown, fewer than 20 atom peaks on a regular lattice may already be sufficient to provide a meaningful ALPD plot from which the correct lattice type and unit cell size can be derived. To achieve the goal of standard crystallographic unit cells, angle constraints were introduced into the code of the developed demonstrator program, which automatically selects the maxima from the plots so that the correct lattice type and 2D unit cell size could be recovered for each of the five possible 2D lattice types. As a tribute to the specific atomic architecture of hcp-type structures, another module has been integrated into the program, which automatically performs a unit cell transformation when 120° hexagonal symmetry is detected. In addition, to extend the capabilities to structures with different atom types, a peak intensity discriminator module has been implemented, allowing the user to select and analyze different sublattices separately. Thus, in its current state, the developed program is a tool capable of analyzing simple, regular lattices, such as those obtained in typical STEM investigations of materials with cubic or hexagonal crystal symmetry, and determining a representative unit cell that can be used for subsequent motif extraction. A

comparison of results for simple 2D structures obtained with a commercial crystallographic image processing (CIP) program [9] and the ALPD code developed in this study has shown that both approaches lead to essentially equivalent results. However, in contrast to the Fourier-based CIP method, which also performs well on slightly disordered structures, a test on structures with randomly displaced atom peaks revealed the strong limitation of the ALPD real-space method to ordered lattices. A further limitation of the ALPD method is that large, more complex unit cells with many atoms may produce complicated ALPD plots due to the limited image size, in which the densely populated lattice directions are difficult to recognize. The CIP method does not have all these limitations. However, if one limits oneself to structures or materials with low structural complexity, such as perovskites or the intermetallic C15 type Laves phases, and the processed image represents a truly periodic structure, the proposed ALPD method is expected to yield similar results to CIP and the variational approach using lattice projections [10]. This was demonstrated using the Nb_7Co_6 test case shown in Figures 20 and 21. However, in contrast to the earlier proposed approach using lattice projections, the method using ALPD plots will always be superior in terms of computational time, since it only needs to analyze the atomic geometry around one representative atom instead of calculating projections with many hundreds or perhaps even thousands of atoms. On the other hand, the ALPD method cannot find a motif where the edges of the 2D unit cells are not populated by atoms, as these are necessary for defining the cell origin and the cell corners. This virtual disadvantage can be eliminated, since the 2D unit cell determined by the ALPD method always has p1 plane group symmetry, and by shifting the cell origin to a higher-order rotation axis that may be present in the projected structure, it is always possible to obtain the 2D unit cell with the higher plane group symmetry. When it comes to processing speed and achieving the highest possible precision, crystallographic image processing is truly unmatched. It delivers averaged results with the perfect plane group symmetry of the undistorted lattice in a matter of seconds, whether dealing with small or large unit cells. The argument of Alhassan et al. that real-space methods are advantageous because they avoid Fourier transform artifacts [10] is not plausible in this context and cannot be confirmed by the present author.

5. Conclusions

It has been shown that the goal of extraction of the basic motif (2D unit cell) from HAADF STEM images of periodic structures can be achieved with great efficiency via angle-resolved lattice population density (ALPD) plots calculated for a single-atom peak in the periodic 2D lattice. An examination of these plots shows that the cell angle of the (primitive) 2D unit cell can be obtained from the angular difference between the largest maxima in the ALPD plot, which correspond to the directions with the highest atom population. In a subsequent step, the vectors of the 2D unit cell axes are calculated from the distances of the nearest atom peaks along these lines to the atom at the origin. By imposing angular constraints that allow only the maxima in the ALPD plot that are consistent with standard crystallographic settings, it was possible to identify the correct 2D unit cell sizes for each of the five existing 2D lattice types. Thus, the real-space method developed here has been shown to be a fast and reliable approach, and it has the notable advantage of requiring much less computational time than a recently proposed method by Alhassan and co-workers, who employed lattice projections [10]. Furthermore, the ALPD method does not require images with many resolved atoms, as 20 or fewer atoms on a periodic lattice can still provide a meaningful ALPD plot, allowing the lattice type to be identified and the 2D unit cell determined. Therefore, the developed method has some potential for use in automated analysis of the periodic lattice in HAADF STEM images of materials with both large and small crystalline regions. It can also be used to determine lattice

characteristics in undistorted regions of a sample for comparison with results from regions of distorted lattice geometry. Another application of ALPD plots could be the automatic detection of symmetries in regular and disordered structures, since hexagonal 2D lattices are characterized by maxima with a typical angle difference of 60°. The same applies to square lattices, which show characteristic maxima with an angle difference of 45° in the ALPD plots.

Funding: The author has carried out this study within Collaborative Research Centre Transregio 188: Damage Controlled Forming Processes (DFG—German Research Foundation, Project-ID 278868966) and SFB 1394: Structural and Chemical Atomic Complexity: From Defect Phase Diagrams to Material Properties (DFG—German Research Foundation, Project-ID 409476157).

Data Availability Statement: The program code and datasets are available on request from the author. All the data and result files used for the article can be found at Zenodo: <https://zenodo.org/records/14826083>.

Conflicts of Interest: The author declares no conflicts of interest.

References

1. Kirkland, E.J. (Ed.) Calculation of Images of Thin Specimens. In *Advanced Computing in Electron Microscopy*; Springer International Publishing: Berlin/Heidelberg, Germany, 2020; pp. 99–141. [CrossRef]
2. Heidelmann, M.; Barthel, J.; Cox, G.; Weirich, T.E. Periodic Cation Segregation in $Cs_{0.44}[Nb_{2.54}W_{2.46}O_{14}]$ Quantified by High-Resolution Scanning Transmission Electron Microscopy. *Microsc. Microanal.* **2014**, *20*, 1453–1462. [CrossRef] [PubMed]
3. Ophus, C. Four-Dimensional Scanning Transmission Electron Microscopy (4D-STEM): From Scanning Nanodiffraction to Ptychography and Beyond. *Microsc. Microanal.* **2019**, *25*, 563–582. [CrossRef] [PubMed]
4. Aroyo, M.I. (Ed.) *International Tables for Crystallography: Space-Group Symmetry: Vol. A*, 2nd ed.; International Union of Crystallography: Chester, UK, 2016; Section 2.1.3.4. [CrossRef]
5. Hammond, C. *The Basics of Crystallography and Diffraction*, 2nd ed.; Oxford University Press: Oxford, UK, 2001.
6. Hovmöller, S. Crystallographic image processing. *Micron Microsc. Acta* **1992**, *23*, 181–182. [CrossRef]
7. Zou, X.; Hovmöller, S. Structure Determination from HREM by Crystallographic Image Processing. In *Electron Crystallography*; Weirich, T.E., Lábár, J.L., Zou, X., Eds.; Springer: Dordrecht, The Netherlands, 2006; Volume 211, pp. 275–300. [CrossRef]
8. Gipson, B.; Zeng, X.; Zhang, Z.Y.; Stahlberg, H. 2dx—User-friendly image processing for 2D crystals. *J. Struct. Biol.* **2007**, *157*, 64–72. [CrossRef]
9. Hovmöller, S. CRISP: Crystallographic image processing on a personal computer. *Ultramicroscopy* **1992**, *41*, 121–135. [CrossRef]
10. Alhassan, A.S.A.; Zhang, S.; Berkels, B. Direct motif extraction from high resolution crystalline STEM images. *Ultramicroscopy* **2023**, *254*, 113827. [CrossRef] [PubMed]
11. Momma, K.; Izumi, F. *VESTA 3* for three-dimensional visualization of crystal, volumetric and morphology data. *J. Appl. Crystallogr.* **2011**, *44*, 1272–1276. [CrossRef]
12. Schindelin, J.; Arganda-Carreras, I.; Frise, E.; Kaynig, V.; Longair, M.; Pietzsch, T.; Preibisch, S.; Rueden, C.; Saalfeld, S.; Schmid, B.; et al. Fiji: An open-source platform for biological-image analysis. *Nat. Methods* **2012**, *9*, 676–682. [CrossRef] [PubMed]
13. Swanson, H. *Circular of the Bureau of Standards No. 539 Volume 1: Standard X-Ray Diffraction Powder Patterns*; National Institute of Standards and Technology: Gaithersburg, MD, USA, 1953; pp. 10–11. [CrossRef]
14. Swanson, H.; Ugrinic, G. *Circular of the Bureau of Standards No. 539 Volume 1: Standard X-Ray Diffraction Powder Patterns*; National Institute of Standards and Technology: Gaithersburg, MD, USA, 1954; p. 45. [CrossRef]
15. Galasso, F.S. *Structure and Properties of Inorganic Solids*, 1st ed.; Pergamon Press: Oxford, UK, 1970; Chapter 7.4; p. 170.
16. Barthel, J.; Weirich, T.E.; Cox, G.; Hibst, H.; Thust, A. Structure of $Cs_{0.5}[Nb_{2.5}W_{2.5}O_{14}]$ analysed by focal-series reconstruction and crystallographic image processing. *Acta Mater.* **2010**, *58*, 3764–3772. [CrossRef]
17. Hovmöller, S.; Sjögren, A.; Farrants, G.; Sundberg, M. Accurate atom positions from electron microscopy. *Nature* **1984**, *311*, 238–241. [CrossRef]
18. Weirich, T.E.; Ramlau, R.; Simon, A.; Hovmöller, S.; Zou, X. A crystal structure determined with 0.02 Å accuracy by electron microscopy. *Nature* **1996**, *382*, 144–146. [CrossRef]

19. Hunt, C.R.; Raman, A. Alloy chemistry of σ (β-U)-related phases—I. Extension of μ-and occurance of μ'-phases in the ternary systems Nb (Ta)-X-Al (X = Fe, Co, Ni, Cu, Cr, Mo). *Z. Für Met.* **1968**, *59*, 701–707.
20. Nakatani, T.; Yoshiasa, A.; Nakatsuka, A.; Hiratoko, T.; Mashimo, T.; Okube, M.; Sasaki, S. Variable-temperature single-crystal X-ray diffraction study of tetragonal and cubic perovskite-type barium titanate phases. *Acta Cryst.* **2016**, *B72*, 151–159. [CrossRef] [PubMed]